Spectroscopy of $Yb^{3+}:CaF_2$: From isolated centers to clusters

V. Petit, P. Camy,* J-L. Doualan, X. Portier, and R. Moncorgé
Centre de Recherche sur les Ions, les Matériaux et la Photonique (CIMAP), UMR 6252 CNRS-CEA-ENSICAEN, Université de Caen, 6 Boulevard Maréchal Juin, 14050 Caen, France
(Received 1 May 2008; published 27 August 2008)

A detailed spectroscopic study of $Yb^{3+}:CaF_2$ is made by using laser selective excitation, low-temperature time-resolved fluorescence, and Raman techniques. Three dominant types of Yb^{3+} isolated ion centers are identified at very low (0.03 at. %) dopant concentration: two of them with cubic and tetragonal symmetries and the third one not clearly identified but likely of trigonal symmetry. Fluorescence decays strongly differ from one site to another. The overall measured positions of the Stark sublevels of the $^2F_{7/2}$ and $^2F_{5/2}$ multiplets are satisfactorily explained by the crystal-field calculations. On the other hand, at higher dopant concentrations, only one dominant class of Yb^{3+} centers occurs which corresponds to some hexameric cluster in which the Yb^{3+} ions site in nearly tetragonal crystal-field environments and whose energy-level positions are discussed and compared with those previously reported in the literature.

DOI: 10.1103/PhysRevB.78.085131 PACS number(s): 78.20.Bh, 78.40.Ha, 78.55.Hx, 71.70.Ch

I. INTRODUCTION

Calcium fluoride (CaF_2), or fluorite, has been known and studied since a long time ago.[1,2] It can be grown by using standard techniques.[3] Trivalent rare-earth ions (RE^{3+}) then easily enter the crystal lattice in substitution for the Ca^{2+} cations, the excess of charge being compensated for by interstitial F^- ions, leading to several kinds of luminescent centers.[4–6] At low RE^{3+} ion concentrations (<0.1 at %), the dopants mainly form isolated centers. These centers can have tetragonal and trigonal symmetries when the charge-compensating F^- anion is located in a cube adjacent to the RE^{3+} dopant or a simple cubic symmetry when no local charge compensation is located nearby.[7–9] On the other hand, at higher RE^{3+} ion concentrations, the dopant ions usually aggregate and form more or less complex clusters.[9–14]

This general description seems rather well accepted. However there are still some controversies concerning the exact positions of the electronic energy levels of the Yb^{3+} isolated luminescent centers which dominate at low dopant concentration and concerning the single-site character and thus the homogeneous nature of the optical transitions within the laser active center which predominate at high dopant concentration.

On the other hand, $Yb^{3+}:CaF_2$ is presently considered as one of the most attractive Yb^{3+}-doped materials for broadly tunable, high power, and short-pulse laser operation[15–17] as well as for bifrequency laser and terahertz wave generation.[18] Interesting results were also obtained by using $Yb^{3+}:CaF_2$ as regenerative amplifier of femtosecond pulses in the millijoule level with very high damage threshold.[19] Even more recently,[20] it was proven that cryogenically cooled materials could lead to even more promising amplification at high power levels.

More reliable spectroscopic data, obtained at low as well as high temperatures with lightly and heavily doped samples, are thus highly desirable. For that purpose, the following study will be divided in two parts. The first one will be devoted to the really low-doped materials, i.e., containing less than 0.05% Yb^{3+} ions, whereas the second one will concentrate more particularly on materials doped with about 2%–6% Yb^{3+} ions, i.e., with the typical dopant concentration of the crystals which are presently developed for the laser applications.

II. MATERIALS AND EXPERIMENTS

$Yb^{3+}:CaF_2$ crystals were grown in our laboratory by using a rf heating Bridgman technique. Ultrapure (5N) CaF_2 and YbF_3 powders were mixed and introduced in a graphite crucible within the growth chamber. To reduce oxygen and water pollution, a good vacuum ($\sim 10^{-5}$ mbar) is achieved before introducing argon into the chamber. No further annealing treatment was applied to the crystals. Good quality crystals with 20 mm length and 11 mm diameter were obtained in this way and the exact rare-earth dopant concentration was measured by using the inductively coupled plasma (ICP) technique. In the following experiments, crystals doped with 0.03–25 at. % Yb^{3+} ions were studied. Room-temperature absorption spectra were obtained by using a PerkinElmer Lambda 9 spectrophotometer, whereas low-temperature (down to 7 K) absorption, emission, and excitation spectra were carried out with the aid of a Jobin Yvon HRS2 monochromator and a closed-cycle He cryogenerator (APD Cryogenics, Inc.). A Hamamatsu model R5108 photomultiplier for near infrared and a Stanford Research Systems model SR830 lock-in amplifier were used to detect and process the fluorescence signals. Wavelength selective excitation in the 950 nm region was provided by a cw Ti:sapphire laser. The Raman spectra were recorded at room temperature by using a Jobin Yvon LabRAM spectrometer and a charge-coupled device (CCD) camera with a resolution of 1 cm^{-1} per pixel.

III. SPECTROSCOPIC PROPERTIES OF LIGHTLY DOPED MATERIALS

We will recall first in Sec. III A all the relevant hypotheses for the Yb^{3+} environments in CaF_2 at low dopant concentration. Then, Sec. III B will deal with a complete de-

TABLE I. Energy-level positions and transition energies reported in the literature for low-doped $Yb^{3+}:CaF_2$ crystals.

Year	Reference	C_{3v} (cm^{-1})	C_{4v} (cm^{-1})	Cubic (cm^{-1})	Other lines (cm^{-1})	Method
1962	32			First excited electronic level located at ~10 384 cm^{-1}	10 322, 10 374	EPR and absorption measurements
1964	24			$^2F_{5/2}$ and $^2F_{7/2}$ multiplet splittings estimated to 630 and 800 cm^{-1}		EPR and crystal-field calculations
1967	28	T_1: 10 188; T_2: 10 995 and 10 257	10 325	10 384	R_1 or R_2: 10 987; R_1 or R_2: 10 271; R_1: 10 241; R_5: 10 377	EPR and absorption measurements
1969	37	T_1: 10 188; T_2: 10 257	10 325	10 384	R_1: 10 271; R_2: 10 241; R_5: 10 377	Zeeman effect on absorption lines
1969	38		10 325	Absorption: 10 845, 10 384; emission: 9737, 9808, 10 384	Absorption: 10 203, 10 190, 10 156; emission: 10 142, 10 080, 10 043	Absorption and emission data
1969	31			$^2F_{7/2}$ sublevels estimated at 0, 580, and 604 and $^2F_{5/2}$ ones at 10 384 and 10 800		ENDOR
1970	32		$^2F_{7/2}$ sublevels estimated at 0, 164, 435, and 440 and $^2F_{5/2}$ ones at 10 325, 10 400, 10 630			ENDOR
1975	41	T_1: absorption: 10 712, 10 378, 10 208∗; emission: 10 128∗, 9883, 9627; T_2: absorption: 11 421, 10 995∗, 10 268∗; emission: 9878, 9140, 8992		Absorption: 10 845∗, 10 384∗; emission: 9737, 9737∗, 9700∗		Theoretical and experimental∗ measurements
2003	21	T_2: absorption: 11 206, 10 995, 10 257; emission: 9647, 9300, 9026				EPR, absorption, and emission spectra
	Our results		bE_1 10 322, bE_2 10 410, bE_3 10 766, bF_1 9744, bF_2 9812, bF_3 9876	cE_1 10 860, cE_2 10 384, cF_1 9600, cF_2 9735, cF_3 10 384		Absorption and emission measurements (see in Figs. 2–6 for nomenclature)

TABLE II. Experimental (a) and theoretical (b) energy-level positions for the Yb^{3+} ions in the cubic, tetragonal, and trigonal sites. All the transitions are both electric and magnetic dipole allowed except for the cubic sites. For these, transitions can only be magnetic dipole allowed except for $\Gamma_7 \leftrightarrow \Gamma_6$, which are also magnetic dipole forbidden.

		O_h		C_{4v}		C_{3v}	
		a	b	a	b	a	b
$^2F_{5/2}$	7			10 766	10 755 (Γ_7)	10 346	10 402 (Γ_6)
	6	10 849	10 846 (Γ_8)	10 410	10 425 (Γ_6)	10 297	10 378 ($\Gamma_4+\Gamma_5$)
	5	10 384	10 384 (Γ_7)	10 322	10 299 (Γ_7)	10 245	10 251 (Γ_6)
$^2F_{7/2}$	4			588	602 (Γ_7)	107	280 (Γ_6)
	3		685 (Γ_6)	520	501 (Γ_6)	83	178 (Γ_6)
	2	649	649 (Γ_8)	456	229 (Γ_6)	42	142 ($\Gamma_4+\Gamma_5$)
	1	0	0 (Γ_7)	0	0 (Γ_7)	0	0 (Γ_6)

scription of the spectroscopic characteristics of the so-called Yb^{3+} isolated ions. No particular investigation will be performed concerning eventual extrinsic luminescent centers which can be formed by Yb^{3+} ions and nearby impurities such as oxygen or hydroxyl ions.[21,22] These centers are usually produced on purpose or nonintentionally because of low-purity raw materials and/or uncontrolled crystal-growth conditions, which is not the case of our high quality single crystals. Such a spectroscopic characterization means conventional absorption measurements as well as laser selective and time-resolved excitation and emission measurements and fluorescence lifetime determinations made at low and high temperatures. The derived positions of the respective Stark sublevels of each multiplet will be then compared to the literature data. Conclusions based on crystal-field calculations will be given in Sec. III C.

A. Literature data on Yb^{3+} ion environments

Since the 1960s, a great amount of works including electron-paramagnetic-resonance (EPR),[21–29] electron-nuclear-double-resonance (ENDOR),[30–34] extended x-ray-absorption fine-structure (EXAFS),[5,35] optical-absorption, and luminescence measurements[9,21,23,28,29,36–40] and crystal-field calculations[24,29,31,32,40–42] have already been carried out to describe the Yb^{3+} ions environments in CaF_2 and to find their respective energy-level positions. From these studies, it appears, first, that two groups of RE^{3+} configurations exist in CaF_2. The first group contains centers with only one RE^{3+} ion. This group is dominant for rare-earth dopant concentrations lower than about 0.05 at. %. The other group is made of clusters with two or more rare-earth ions and becomes clearly dominant for dopant concentrations higher than about 0.1%.[5]

A sum-up of the line positions reported in the literature and concerning the Yb^{3+} centers in CaF_2 at low dopant concentrations is presented in Tables I and II. Even if everything has not been yet fully demonstrated, the possible configurations for the RE^{3+} ions in calcium fluoride at low doping concentrations are now relatively well admitted.[43,44] During crystal growth, some of the trivalent RE^{3+} ions thus substitute for the divalent calcium ions and site in cubic (O_h) environments.[4] In this situation, interstitial fluorine ions (F_i^-) compensate for the difference in charge but far from the considered RE^{3+} ions. On the contrary, these interstitial fluorine ions (F_i^-) may also be located in the vicinity of the RE^{3+} ions, which then results in the existence of two other kinds of RE^{3+} ion environments of tetragonal (C_{4v}) and trigonal (C_{3v}) symmetries. These three types of configurations can be clearly detected optically only at very low dopant concentrations and, as mentioned above, to avoid the appearance of other more complicated centers, by working with high quality crystals free of any other unwarranted impurities and defects, which was rarely the case in the past. Moreover, it is worth noting that the proportion of each luminescent center does not depend only on the radius of the considered rare-earth ion. Indeed, it may depend also on the growing process since, due to the F^- ion mobility, the local environment of the RE^{3+} ion may depend on the thermal history (cooling and annealing processes) of each crystal.[40,41]

1. Yb^{3+} *ions in sites of cubic symmetry*

The electronic ground-state multiplet ($^2F_{7/2}$) of Yb^{3+} ions in cubic site symmetry should split into three components, whereas their excited one ($^2F_{5/2}$) should split into two sublevels.[23] As a matter of fact, an intense cubic absorption line located at about 962.98 nm ($\sim$10 384 cm^{-1}) was indeed first reported by Low[36] in 1962 and firmly confirmed later on by Kirton and co-workers.[28,37] That line was found to be the zero line and this was corroborated by all the following studies.[31,38,41] EPR and field parameters calculations made by Weber and Bierig[24] also allowed estimation of the overall crystal-field splitting of the $^2F_{5/2}$ multiplet to $\sim$630 cm^{-1} and that for the $^2F_{7/2}$ ground state to $\sim$800 cm^{-1}. However it was admitted that further work was necessary to confirm the measurements and verify the interpretations. Voron'ko *et al.*[38] finally proposed a complete set of cubic lines from spectroscopic measurements. They found low-temperature absorption lines, thus excited energy levels, at 922 nm (10 845 cm^{-1}) and 963 nm (10 384 cm^{-1}). They also reported a fluorescence line at 963 nm, thus corresponding to the reverse transition of the previous one, and two other lines at 1019.5 nm (9808.7 cm^{-1}) and 1027 nm (9737.1 cm^{-1}).

The positions of these two lines would indicate $^2F_{7/2}$ multiplet sublevels at about 574 and 612 cm^{-1}, respectively. Only the latter, however, could be unambiguously assigned to the same cubic center.

2. Yb^{3+} *in sites of noncubic symmetry*

C_{4v} and C_{3v} symmetry centers respectively involve a fluorine ion F^- in the nearest-neighbor or the next-nearest-neighbor interstitial sites for charge compensation. The symmetry is axial about the cubic axes for C_{4v} and axial about the diagonal of the cube for C_{3v}.

ENDOR experiments identified the Yb^{3+} ions in the tetragonal sites of C_{4v} symmetry rather unambiguously. They allowed an estimation of the crystal-field parameters and of the energy-level positions.[32] However, it is interesting to note that, to the best of our knowledge, only two papers reported on the observation of optical lines belonging to Yb^{3+} centers of C_{4v} symmetry.[28,38] Moreover, in these papers only one absorption transition was observed at about 968.5 nm (10 325 cm^{-1}). This illustrates the fact that it is not obvious to identify this type of lines by classical optical measurements.

Some lines reported by McLaughlan and Newman[26] were also assigned to trigonal sites. The exact nature of these sites is different, however, from that of trigonal sites of C_{3v} symmetry, as described above. Indeed, in most of the studies, the so-called T_1, T_2, or T_3 trigonal sites (see Ref. 4) involve, in fact, trigonal centers associated with nearby oxygen impurities. The most frequent one is the trigonal T_2 center, where a charge-compensating O^{--} ion substitutes for one of the eight F^- ions. Baker and Davies[41] thus reported crystal-field parameters calculated for several types of trigonal centers to account for EPR results. This type of sites was also studied in detail more recently by EPR and optical measurements.[21] However there again the experimental optical signature of a single type of C_{3v} Yb^{3+} center involving an Yb^{3+} ion and a fluorine ion in the next-nearest-neighbor interstitial site is not clearly established.

B. Spectroscopy of low-concentration Yb^{3+}:CaF_2 crystals

This spectroscopic analysis was mainly performed with a 0.03 at. % Yb^{3+}–doped CaF_2 crystal. At that concentration and with the growing process used, the proportion of clusters is negligibly small; the spectroscopic signatures of the respective Yb^{3+} isolated centers were thus easier to identify. The results obtained for each center, their spectra, and associated energy-level positions are reported and discussed in the following paragraphs.

1. Yb^{3+} *ions in sites of cubic symmetry*

It was suggested in the past[28,37,38,41] that the transition line reported in both the low-temperature absorption and emission spectra at about 962.98 nm (10 384 cm^{-1}) was the "zero line" (transition between the lowest components of each multiplet) for the Yb^{3+} ions in cubic symmetry. This is confirmed by our own fluorescence and excitation spectra recorded at 7 K and reported in Fig. 1. As expected, four purely electronic (electric dipole forbidden but magnetic dipole allowed) spectral lines could be identified and attributed to Yb^{3+} ions in a cubic symmetry environment: two intense excitation lines labeled cE_1 (10 850 cm^{-1}) and cE_2 (10 384 cm^{-1}) and two emission lines labeled cF_1 (9735 cm^{-1}) and cF_3 (10 384 cm^{-1}). The other lines found in the emission spectra are assigned to vibronic satellites and residuals of electronic lines associated with other types of Yb^{3+} centers. From these data, the energy-level scheme reported in Fig. 2 is suggested.

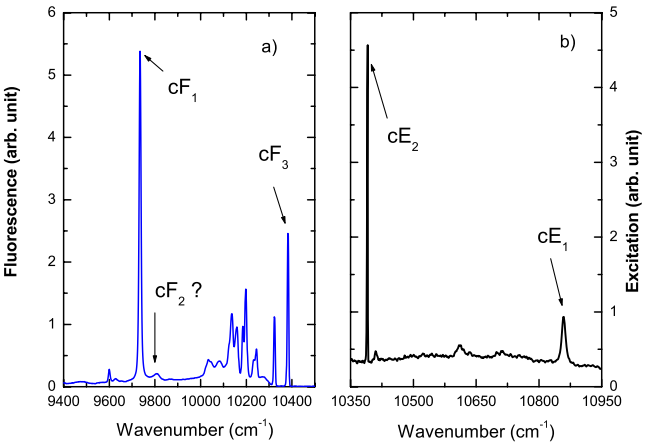

FIG. 1. (Color online) 7 K emission (a) and excitation (b) spectra of the Yb^{3+} cubic sites in CaF_2 obtained by exciting the samples at 921 nm (10 849 cm^{-1}) and by monitoring the emission at 1027 nm (9736 cm^{-1}), respectively.

The validity of such an assignment was primarily checked by performing fluorescence lifetime measurements. These measurements indeed proved that both the cF_1 and the cF_3 emission lines were associated with the same emitting level and the common emission lifetime of 10.5 ms. The assignment was also checked by juxtaposing the emission over the absorption spectrum around the common cF_3 and cE_2 zero-line transitions and by noting that no coincidence of any other lines which could be assigned to some vibronic sidebands associated with some specific phonon energy actually occurred.

2. Yb^{3+} *ions in sites of tetragonal symmetry*

Seven lines should be observed at low temperature for C_{4v} symmetry centers since the ground and the excited multiplets

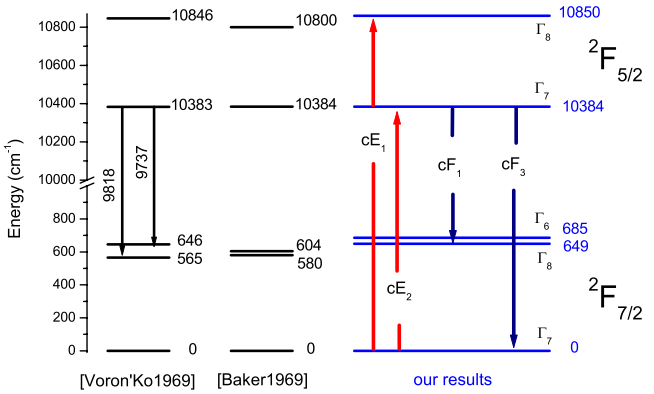

FIG. 2. (Color online) Energy-level scheme (in cm^{-1}) for the Yb^{3+} cubic centers in CaF_2

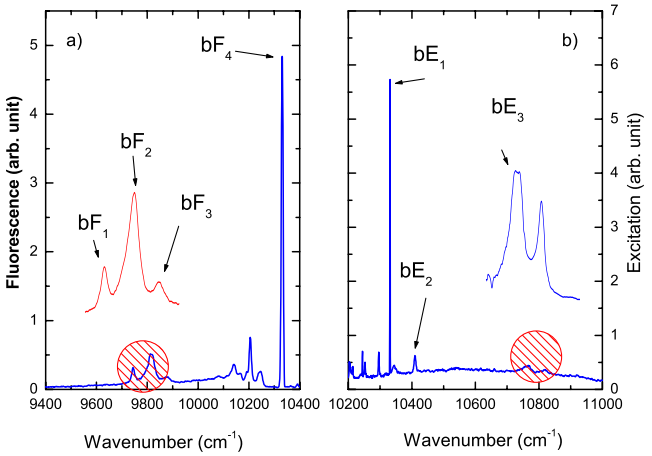

FIG. 3. (Color online) 7 K emission (a) and excitation (b) spectra of the Yb^{3+} tetragonal (C_{4v}) sites in CaF_2 obtained by exciting the sample at 928 nm (10 766 cm^{-1}) and by monitoring the emission at 1019 nm (9813 cm^{-1}), respectively.

$^2F_{7/2}$ and $^2F_{5/2}$ should split into four and three levels, respectively.[24] Among all the data which can be found in the literature, only one absorption line corresponding to a C_{4v} symmetry was reported by Kirton and McLaughlan[28] and by Voron'ko *et al.*[38] It is located at about 10 325 cm^{-1}. This line was assigned to the zero line (ZL) of these C_{4v} centers. As expected, emission and excitation measurements allowed us to observe seven lines; they are shown in Fig. 3. The intense line located at around 10 332 cm^{-1} and appearing both in the emission and the excitation spectra (lines bE_1 and bF_4) is unambiguously assigned (though slightly shifted compared to the one reported in the literature) to the ZL for the tetragonal sites. The other excitation lines located at 10 766 and 10 410 cm^{-1} and labeled bE_3 and bE_2 as well as the emission lines at 9876, 9812, and 9744 cm^{-1} and labeled bF_3, bF_2, and bF_1, respectively, present much lower intensities. The energy-level scheme deduced from these data is reported in Fig. 4. From these measurements, the splittings of the $^2F_{5/2}$ and $^2F_{7/2}$ multiplets are 434 and 588 cm^{-1}, respectively. To confirm these experimental results, fluorescence decays were measured by exciting selectively these C_{4v} centers. The same fluorescence lifetime of about 8 ms

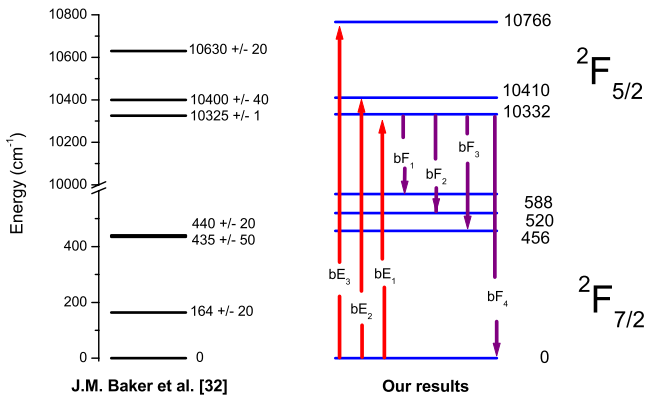

FIG. 4. (Color online) Energy-level scheme (in cm^{-1}) for Yb^{3+} tetragonal centers in CaF_2.

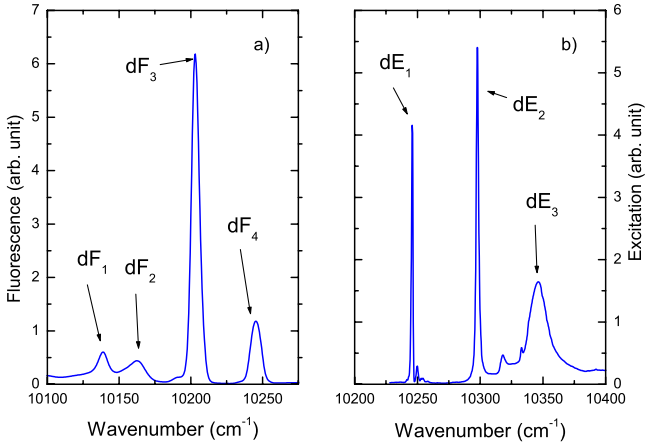

FIG. 5. (Color online) 7 K emission (a) and excitation (b) spectra of the Yb^{3+} trigonal (C_{3v}) sites in CaF_2 obtained by exciting the sample at 971 nm (10 298 cm^{-1}) and by monitoring the emission at 980.4 nm (10 200 cm^{-1}), respectively.

(+/−10%) was then obtained for the four emission lines (bF_1, bF_2, bF_3, and bF_4).

3. Yb^{3+} *ions in sites of trigonal symmetry*

At low temperature, seven levels (and seven lines) again are expected for the Yb^{3+} ions in sites of C_{3v} symmetry: four and three for the ground and excited multiplets $^2F_{7/2}$ and $^2F_{5/2}$,[24] respectively. By investigating all the different emission and absorption spectra, four lines in emission at about 10 245, 10 203, 10 162, and 10 138 cm^{-1} and three lines in absorption at about 10 245, 10 297, and 10 346 cm^{-1} (see in Fig. 5) were identified. All the fluorescence lines decay with the same time constant of 2.1 ms. The corresponding Yb^{3+} centers could not be associated with any of the trigonal sites discussed in the literature. These centers indeed were associated with either nearby oxygen[21,28,37,41] or hydrogen[45] impurities. By comparison with these results, it was found that our samples did not contain any such unwanted impurities, so that it was concluded that the detected center could be a "pure" trigonal center, formed just with one Yb^{3+} ion and nine nearby fluorine ions. The following crystal-field calculations, though not completely unfavorable, will prevent us, however, to be so sure about such an interpretation. In the end, it is worth noting that by using crystals with different levels of ytterbium concentration, it was observed that these assumed C_{3v} centers disappeared when the Yb^{3+} concentration was increased beyond about 0.1 at. % Yb^{3+} (see in Fig. 7). This may explain why there was so much confusion in the past concerning that type of centers.

C. Crystal-field calculations

Ab initio crystal-field calculations rarely give satisfactory results. Moreover, in the case of the Yb^{3+} ion, as there are only two multiplets and thus a reduced number of energy levels, it is difficult, even illusory (except for a cubic crystal field which depends on only two parameters), to get reliable crystal-field parameters by using a fitting procedure.

Consequently, in the following, to confirm our previous assignments, we examined the cubic symmetry and the tetragonal and trigonal symmetries separately. In the case of the cubic symmetry, we started from the (Stevens-type) crystal-field parameters proposed in the past and adjusted them to fit our own data. For the lower symmetries, we compared our data with the energy-level positions which can be derived from the crystal-field parameters obtained in the literature with other ions such as Eu^{3+} (Ref. 8) and Tm^{3+}.[7] This is a rough procedure but it should give an idea of the energy-level scheme of each kind of centers.

For the Yb^{3+} ions in the cubic sites, first, the analytical expressions used in the past by Low,[23] Kiro and Low,[33] and Baker *et al.*[31] to account for their EPR, optically detected magnetic resonance (ODMR), or optical data led to the Stevens-type crystal-field parameters

$$b_4(\mathrm{L,B}) \approx 51.6 \text{ and } 44.5 \text{ cm}^{-1}$$

and

$$b_6(\mathrm{L,B}) \approx 6.39 \text{ and } 7.02,$$

respectively, where the $b_4(\mathrm{L,B})$ and $b_6(\mathrm{L,B})$ parameters used by Low and Baker *et al.* are related to those used by Weber and Bierig[24] by $b_4(\mathrm{L,B})=\frac{7}{3}b_4(\mathrm{W})$ and $b_6(\mathrm{L,B})=b_6(\mathrm{W})$.

Converting then these Stevens-type parameters into Wybourne ones, as they appear when the crystal-field Hamiltonian is expressed as[46,47]

$$H_{\mathrm{CF}} = \sum_{k,q} B_q^k \sum_i C_q^k(i), \tag{1}$$

thus, by writing

$$B_4^0 = -33b_4(\mathrm{L,B}) \text{ and } B_6^0 = \frac{429}{5}b_6(\mathrm{L,B}),$$

with

$$B_4^4 = \sqrt{\frac{5}{14}}B_4^0 \text{ and } B_6^4 = -\sqrt{\frac{7}{2}}B_6^0,$$

the above b_4 and b_6 values lead to B_4^0 values in the $1468-1703$ cm^{-1} range and B_6^0 values in the $529-602$ cm^{-1} range.

This is in good agreement with the B_4^0 and B_6^0 parameters which we have found by using a standard crystal-field calculation procedure[46,47] based on the above Hamiltonian [Eq. (1)] and by fitting our own data, i.e.,

$$B_4^0 \approx -1710 \text{ cm}^{-1} \text{ and } B_6^0 \approx 550 \text{ cm}^{-1}.$$

The corresponding calculated energy levels are reported and compared with the experimental ones in Table II.

It is worth noting here that only the ground-state sublevels at 0 and 649 cm^{-1} and the excited ones at 10 384 and 10 850 cm^{-1} can be observed, in fact, by recording absorption and emission spectra. The level at 685 cm^{-1} is associated, indeed, with a Γ_6 irreducible representation, whereas all the other energy levels are associated with a Γ_7 or a Γ_8 representation. The consequence is that all the optical transitions involving this Γ_6 energy level are both electric and magnetic dipole forbidden.

Concerning the Yb^{3+} ions in the tetragonal sites, the positions of the energy levels are obtained, as above, by using the crystal-field parameters expressed in the Wybourne notation. In this case, however, the parameters are simply derived from those obtained by Strickland and Jones[7] in the case of the Tm^{3+} ions but modified by using the expressions[47]

$$B_q^k(\mathrm{Yb}^{3+}) = \frac{\rho_k(\mathrm{Yb}^{3+})}{\rho_k(\mathrm{Tm}^{3+})} B_q^k(\mathrm{Tm}^{3+}), \tag{2}$$

where the radial factors have been given by Ferrier *et al.*,[46] and by writing, to account for the different notations used in Ref. 7,

$$B_0^2 = B_A^2, \quad B_0^4 = B_c^4 + B_A^4, \quad B_4^4 = \sqrt{\frac{5}{14}}B_c^4 - \sqrt{\frac{7}{10}}B_A^4,$$

$$B_0^6 = B_c^6 + B_A^6, \quad B_4^6 = \sqrt{\frac{1}{14}}B_A^6 - \sqrt{\frac{7}{2}}B_c^6.$$

In this way, the crystal-field parameters

$$B_0^2 = 567 \text{ cm}^{-1}, \; B_0^4 = -686.5 \text{ cm}^{-1}, \; B_0^6 = 827.5 \text{ cm}^{-1},$$

$$B_4^4 = -957 \text{ cm}^{-1}, \text{ and } B_4^6 = -768 \text{ cm}^{-1}$$

and the energy-level positions reported in Table II are found. Considering the roughness of the procedure, the agreement between the theoretical and experimental values is rather satisfactory.

The same procedure was applied for the assumed trigonal centers, in that case by using again the parameters reported by Strickland and Jones,[7] and transforming then in our notation by writing

$$B_0^2 = B_A^2, \quad B_0^4 = B_c^4 + B_A^4, \quad B_3^4 = \sqrt{\frac{10}{7}}B_c^4 - \sqrt{\frac{7}{40}}B_A^4,$$

$$B_0^6 = B_c^6 + \hat{B}_A^6,$$

$$B_3^6 = \sqrt{\frac{11}{42}}B_A^6 - \sqrt{\frac{35}{96}}B_c^6 + \sqrt{\frac{160}{1029}}\hat{B}_A^6$$

$$\text{and } B_6^6 = \sqrt{\frac{77}{192}}B_c^6 - \sqrt{\frac{176}{1029}}\hat{B}_A^6 + \sqrt{\frac{5}{21}}B_A^6.$$

In this way, by correcting for the little inversion made in Table IX of Ref. 7 between the values for $\hat{B}_A^6$ and B_A^6, the crystal-field parameters

$$B_0^2 = 231.5 \text{ cm}^{-1}, \; B_0^4 = -323.5 \text{ cm}^{-1},$$

$$B_0^6 = 137.5 \text{ cm}^{-1}, \; B_3^4 = -199 \text{ cm}^{-1},$$

$$B_3^6 = -704 \text{ cm}^{-1} \text{ and } B_6^6 = 272.5 \text{ cm}^{-1}$$

and the energy-level positions reported in Table II are obtained. Although the agreement between the semitheoretical

and the experimental values remains rather satisfactory for the excited-state sublevels, it is definitely not for the ground-state ones.

At this step, it is worth noting that the overall crystal-field splittings of about 100 cm^{-1} for the ground and excited multiplets associated with these trigonal sites are significantly weaker, by about a factor of 5, than in the case of the tetragonal and cubic sites. At first sight, this looks rather surprising but not radically unexpected. Going back, indeed, to the results obtained in the past by Strickland and Jones[7] in the case of doped CaF_2, the ground and excited multiplets splittings range between about 60 and 380 cm^{-1} for the trigonal sites and between 180 and 690 cm^{-1} for the tetragonal ones, which means a factor of 2–3. Consequently, though it is certainly difficult to definitely assign what was interpreted above as Yb^{3+} trigonal centers to real C_{3v} symmetry Yb^{3+} sites, such an interpretation cannot be completely discarded. For that reason, we shall refer in the following to the "assumed trigonal" sites.

IV. SPECTROSCOPIC PROPERTIES OF HEAVILY DOPED CRYSTALS

Different sort of clusters, depending on the thermal history of the crystal and on the size of the rare-earth ions, have been suggested in fluorite. Based on two to six or more ions, rare-earth clusters represent the main situation for dopant concentrations exceeding about 0.5%.[11,12] The stability of the different clustered structures was calculated by Catlow *et al.*[5] and it was shown that the probabilities of forming a given cluster are not the same for all the rare-earth ions. EXAFS measurements confirmed, for example, that RE^{3+} ions with small radii such as Yb^{3+} or Tm^{3+} have the tendency to form large six ion clusters—hexamers—rather than dimers or tetramers[5] and that these RE^{3+} ions inside these clusters have cubo-octahedral environments.[11] More recently, EPR measurements and computer simulations showed that Er^{3+}, Tm^{3+}, and Yb^{3+} are organized in hexameric clusters, RE_6^{3+}-F_{37}^- type, embedded in the fluorite lattice.[13,14] As these studies mainly dealt with EXAFS and EPR measurements and only very few and nonconverging data were reported on the optical spectroscopy of these centers, the present section aims to fill the gap by bringing detailed spectroscopic data about the luminescent centers in Yb^{3+}:CaF_2 when Yb^{3+} ions do not site in cubic, tetragonal, or trigonal isolated environments, as ascribed previously, but gather and form clusters.

A. Appearance of lasing centers above 0.1 at. % Yb^{3+}

The first obvious signature of the local changes in the rare-earth environment is the shape of the transmission spectra recorded at low temperature. Figure 6 shows such transmission spectra at a temperature of 7 K for different Yb^{3+} concentrations. The spectra have been normalized by the thickness and the concentration of the samples. Up to 0.115%, the relative intensities of the observed lines change but they remain well structured. Among the observed transitions, those corresponding to RE^{3+} in cubic (O_h), tetragonal (C_{4v}), and trigonal (C_{3v}) sites have been previously identified:[6] 10 332 cm^{-1} (ω) and 10 410 cm^{-1} (δ) for the C_{4v} centers, 10 245 cm^{-1} (β) and 10 297 cm^{-1} (γ) for the C_{3v}, and 10 384 cm^{-1} (λ) for the O_h.

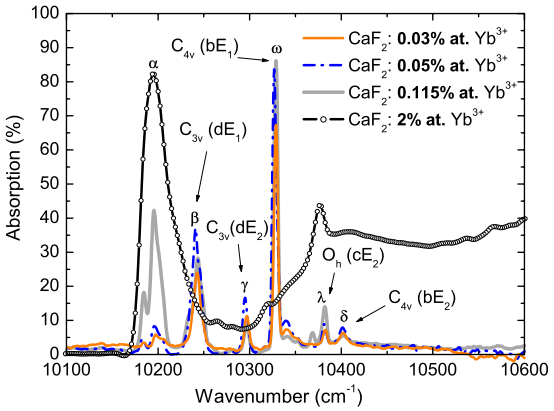

FIG. 6. (Color online) Absorption spectra for samples with various Yb^{3+} concentrations at $T=7$ K (spectra normalized by the thickness and the Yb^{3+} concentration of the samples).

For doping levels of about 2% and higher, the spectrum broadens and some lines disappear. This is the case of the C_{4v} ($\omega-10\,332$ cm^{-1}) and the C_{3v} lines ($\beta-10\,245$ cm^{-1} and $\gamma-10\,297$ cm^{-1}). However, a major contribution around 10 200 cm^{-1}, labeled α in the figure, appears and grows as the Yb concentration increases.

The evolution of the relative intensities of the transmission lines attributed to the different centers versus the ytterbium concentration is presented in Fig. 7. The intensities of these lines have been previously normalized by the thickness as well as the Yb concentration of the studied crystals. For Yb^{3+} concentrations between 0.03% and 0.115%, the proportion of the C_{3v} and C_{4v} isolated centers decreases, whereas the cubic line λ slightly increases and line α becomes more and more dominant over all the others. Figure 8 displays the absorption spectrum obtained with a sample doped with 2 at. %. This result corroborates the optical measurements of Voron'ko *et al.*,[38] according to which cubic centers still exist at relatively high dopant concentration. At higher concentration, however, the structure associated with these cubic centers (line λ) also progressively disappears inside the broad vibronic sideband of the hexameric centers.

B. Single-site character of the Yb^{3+} lasing center

1. Low-temperature emission measurements

Emission spectra (displayed in Fig. 9) were registered by exciting a 2%Yb^{3+}:CaF_2 crystal at different wavelengths across the absorption spectrum (as reported in Fig. 8): α_1 at 10 190 cm^{-1}, α_2 at 10 384 cm^{-1} (O_h center excitation), α_3 at 10 688 cm^{-1}, and α_4 at 10 885 cm^{-1}. The spectrum reveals one isolated narrow line located around 10 200 cm^{-1} and other sharp peaks and broad bands at higher wavelengths. The intense and narrow line has been previously observed in the absorption spectrum and can be safely associated with an optical transition within the Yb^{3+} centers which appear at high doping levels. At the same time, it can be observed that whatever the excitation wavelength is, the

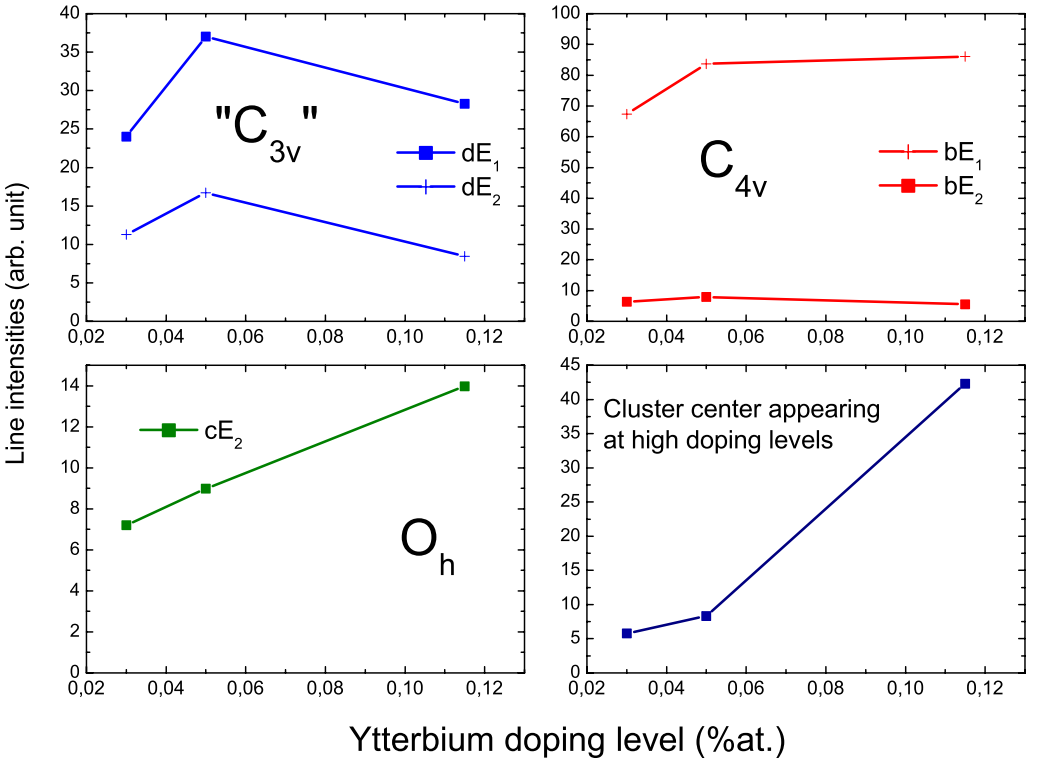

FIG. 7. (Color online) Relative intensities of the transitions assigned to trigonal (C_{3v}) (a), tetragonal (C_{4v}) (b), cubic (O_h) (c), and cluster centers (d).

obtained spectra present the same shape and particularly no signature of exalted cubic lines. From this result, it can be already concluded that only one kind of Yb^{3+} centers emits at such doping level and that even at low temperature, there is no trace of multisite structures (or they are negligible).

2. Room-temperature spectroscopic measurements

Figure 10 shows room-temperature absorption spectra registered with samples doped with 2, 5.5, 6, 9, and 12 at. % Yb^{3+} ions. As can be seen, no influence of the Yb^{3+} concentration on the shape of the spectra can be noticed.

Figure 11 shows in turn the room-temperature emission spectra registered with samples doped with 0.8, 5, 15, and 25 at. % Yb^{3+} ions. Here again except for the peak around 10 200 cm^{-1}, which is noticeably attenuated at the higher doping levels by the classical reabsorption effect,[48] the overall shape of the spectra remains the same, indicating again that there is only one type of majority cluster centers for the Yb^{3+} ions responsible for the luminescent and thus the lasing properties of the $Yb:CaF_2$ system when the dopant concentration exceeds a few percent.

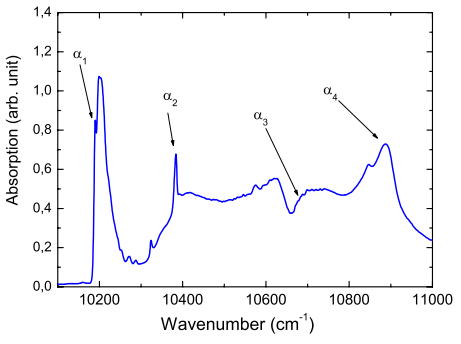

FIG. 8. (Color online) Low-temperature (7 K) absorption spectrum of a 2 at. % $Yb^{3+}:CaF_2$ crystal

C. Assignment of the energy levels corresponding to the main Yb clusters

Only two papers really addressed that difficult question. By studying the low-temperature absorption and emission spectra as well as the fluorescence lifetimes of each of the

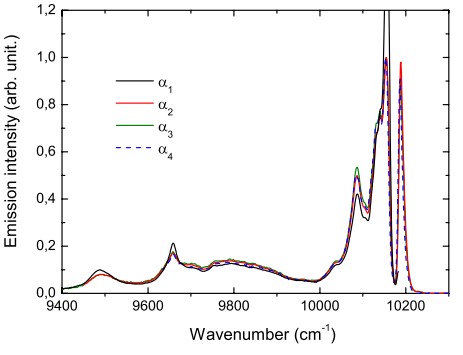

FIG. 9. (Color online) Low-temperature (7 K) emission spectra of a 2 at. % $Yb^{3+}:CaF_2$ crystal for different excitation wavelengths (see in Fig. 8).

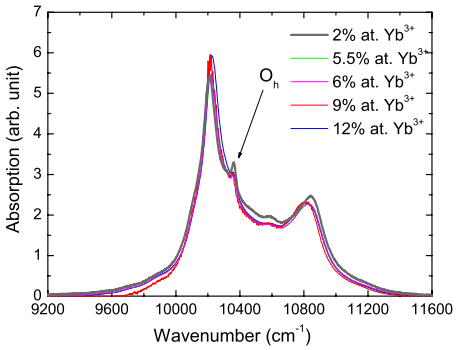

FIG. 10. (Color online) Room-temperature absorption spectra of heavily doped Yb^{3+}:CaF_2 crystals.

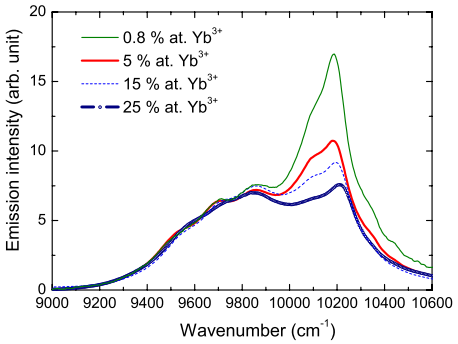

FIG. 11. (Color online) Room-temperature emission spectra of heavily doped Yb^{3+}:CaF_2 crystals obtained after 10 800 cm^{-1} excitation.

individual emission lines in samples doped with 0.1–3 at. % Yb^{3+} ions, Voron'ko *et al.*[38] concluded the existence of an Yb^{3+} site corresponding to a low-symmetry weak-crystal-field environment and energy-sublevels position at 0, 46, 109, and 146 cm^{-1} for the ground multiplet $^2F_{7/2}$ and 10 189 and 10 202 cm^{-1} for the $^2F_{5/2}$ metastable one. They also invoked vibronic sidebands associated with vibrational frequencies of 330, 410, 495, and 650 cm^{-1}. Ito *et al.*[39] made a similar analysis with samples doped with 0.5, 5, and 30 at. % Yb^{3+} ions. They also referred to some Raman spectra indicating that only one peak occurs around 320 cm^{-1}. Their finally proposed energy-sublevel positions at 0, 103, 518, and 675 cm^{-1} for the ground multiplet and at 10 200, 10 384, and 10 870 cm^{-1} for the excited one. These results clearly differ from each other (Table III). They are obviously some misinterpretations which likely come from two types of confusions: confusions between purely electronic transitions and vibronic sidebands and confusions with electronic transitions pertaining to different kinds of centers. The energy-level position reported by Ito *et al.*[39] at 10 384 cm^{-1}, for example, is typical of the Yb^{3+} cubic centers. This is the reason why it was decided here to reanalyze that question but by recording low-temperature laser excitation, emission, and Raman spectra as well as fluorescence lifetimes with samples doped with low and intermediate concentrations of 0.05% and 0.115% Yb^{3+} ions. According to the results given in Fig. 6, indeed, at low temperatures and low dopant concentrations, it is still possible to distinguish between the different centers. Above about 0.5% Yb^{3+}, as was made by Ito *et al.*,[39] the contribution of the Yb^{3+} clusters dominates and the lines broaden so much that it becomes too difficult to discriminate between the purely electronic and vibronic transitions.

1. Low-temperature emission and excitation data

The emission spectra were obtained by pumping the crystal at 10 200 cm^{-1} (see in Fig. 8). The excitation ones were registered by monitoring the emission intensity at about 10 140 cm^{-1}—the peak associated with the clusters (see in Fig. 9).

At the lowest concentrations, the emission spectra (see in Fig. 12) reveals a common line located at 10 190 cm^{-1} accompanied by another one around 10 140 cm^{-1} and made of three overlapping contributions labeled γ_4, γ_5, and γ_6 at 10 143, 10 139, and 10 131 cm^{-1}. The first line was already identified by Voron'ko *et al.*[38] (see above) as the zero line associated with the majority sites appearing at high dopant concentration, thus the Yb clusters. Consequently, as the other group of lines located around 10 140 cm^{-1} roughly follows the same behavior with the dopant concentration, these lines also probably participate in the same type of Yb clusters. On the other hand, the question remains about the origin of the lines growing with the dopant concentration and labeled γ_2, γ_3, and γ_7 located around 10 159, 10 152, and 10 080 cm^{-1}.

TABLE III. Positions of the Yb clusters' energy levels.

			Ref. 39		Ref. 38	This study
	Electronic levels	0.5 mol %	5 mol %	30 mol %	>0.455 at. %	
$^2F_{5/2}$	7	10 881 [a]	10 870 [a]	10 837 [a]		~10 580
	6	10 390 [b]	10 384 [b]	10 379 [b]	10 202	~10 300
	5	10 199	10 204	10 230, 10 246	10 189	10 190, 10 205, 10 212
$^2F_{7/2}$	4	689[a]	675[a]	593[a]	146[a]	~530
	3	532[a]	518[a]	462[a]	109[a]	~110
	2	113	103	88	46	47, 50, 46
	1	0	0	0	0	0

[a]Vibronic sidebands.

[b]Lines previously assigned to cubic centers.

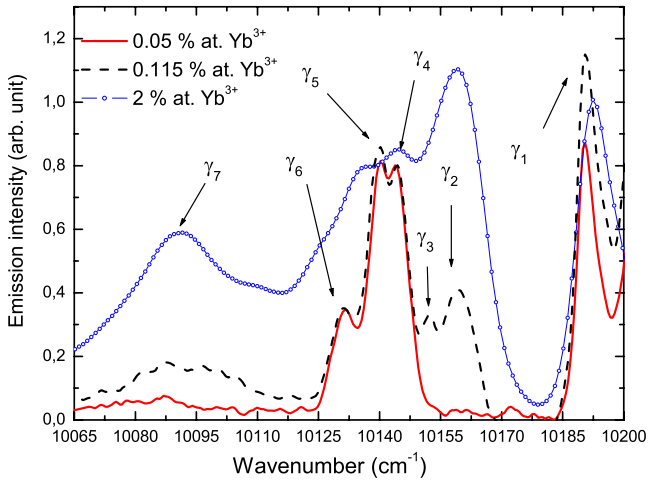

FIG. 12. (Color online) High-energy portion (see in Fig. 9) of the emission spectra of the Yb^{3+} clusters obtained at 7 K by pumping at 10 200 cm^{-1} (normalization made at 10 140 cm^{-1}).

As shown in Fig. 13, where the low-energy portion of the excitation spectra obtained by monitoring the emission around 10 140 cm^{-1} (an emission which likely comes from the Yb^{3+} clusters) is reported, contributions arise both from the excitation of these centers and from the isolated ones. We indeed find the already identified excitation line cE_2 of the O_h symmetry centers at about 10 384 cm^{-1}, the excitation line bE_1 of the $C_{4v}s$ symmetry at 10 332 cm^{-1} and the lines dE_1, dE_2, and dE_3 of the $C_{3v}s$ symmetry at 10 245, 10 297, and 10 346 cm^{-1}. We also clearly distinguish a group of three lines with about the same intensity ratio, a first one labeled Γ_1 around 10 190 cm^{-1}, which is the already identified zero line of the Yb^{3+} clusters, and two others labeled Γ_2 and Γ_3 around 10 205 and 10 212 cm^{-1}.

2. Raman spectra and vibronic sidebands

Some complementary data were obtained first by recording the Raman spectra of samples with increasing dopant

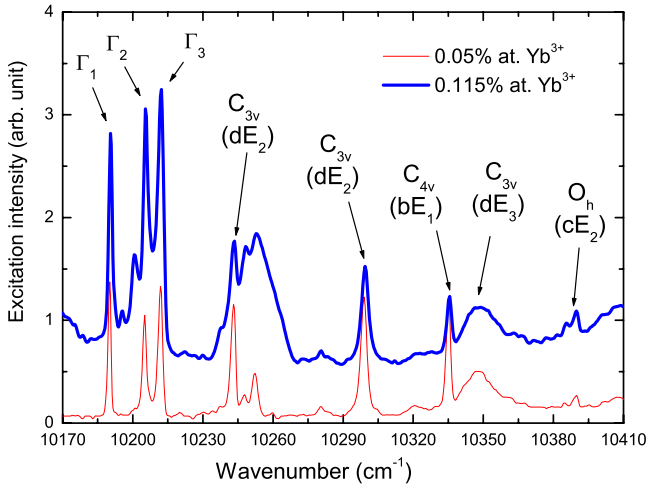

FIG. 13. (Color online) Low-energy portion (see in Fig. 7) of the excitation spectra associated with the Yb^{3+} clusters at 7 K (emission monitored at 10 140 cm^{-1}).

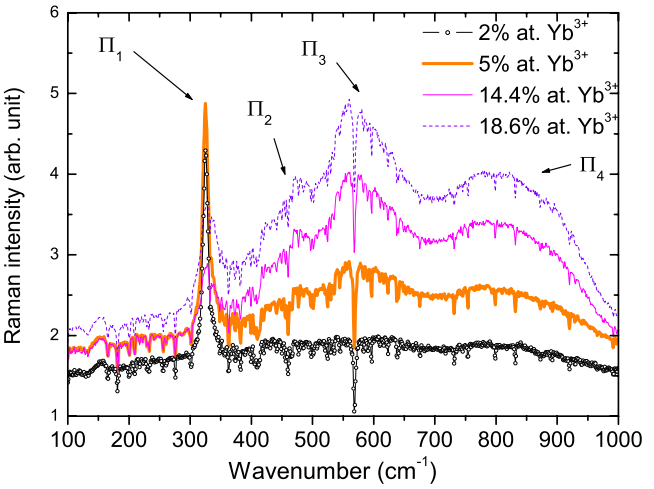

FIG. 14. (Color online) Raman spectra (excitation at 633 nm) of highly concentrated Yb^{3+}:CaF_2 single crystals.

concentrations, as displayed in Fig. 14, and by comparing the overall spectral shapes of the emission and excitation spectra which are obtained at high dopant concentrations, as reported in Fig. 15. As indicated by the Raman spectra, there is a sharp peak around 325 cm^{-1}, which is characteristic of the lattice phonon mode of the pure CaF_2 single crystal, as well as concentration dependent broad bands peaking around 460, 570 and 800 cm^{-1}, which can be probably assigned to local phonon modes associated with the Yb^{3+} clusters. As a matter of fact, when comparison is made between the emission and excitation spectra, by folding one over the other around the position of the zero line at 10 190 cm^{-1}, as shown in Fig. 15, clear coincidences can be seen between vibronic sidebands located around 430, 530, and 695 cm^{-1}, thus in rather good agreement with the Raman data.

3. Discussion of the results

From these emission and excitation spectra and more particularly from the positions of the emission lines γ_1, γ_4, γ_5,

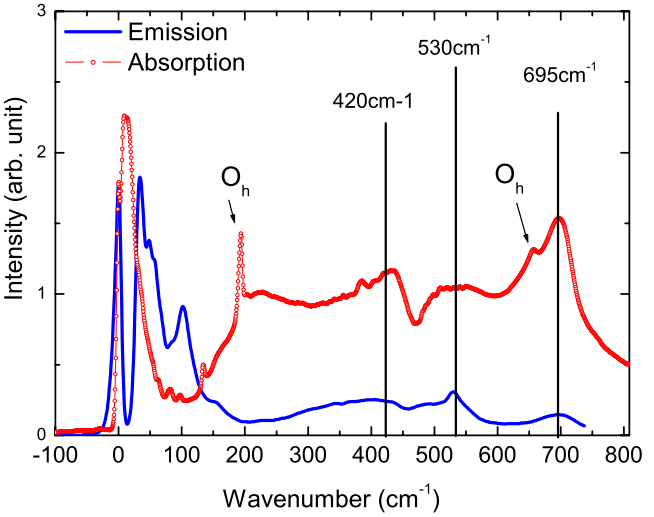

FIG. 15. (Color online) Absorption and emission spectra at T =7 K for a 2%Yb^{3+}:CaF_2 single crystal, folded around the zero-line position at 10 190 cm^{-1}.

and γ_6 and of the excitation lines Γ_1, Γ_2, and Γ_3, it is thus possible to give the energy-level scheme of the Yb^{3+} clusters with groups of levels at about 46, 50, and 58 cm^{-1} for the $^2F_{7/2}$ ground multiplet and 10 190, 10 205, and 10 212 cm^{-1} for the $^2F_{5/2}$ one. Such groups of levels would correspond to optical transitions within Yb^{3+} belonging to the same cubo-octahedral cluster but sitting inside different antiprisms. Works by Ness *et al.*,[11] Bevan *et al.*,[12] and then by Laval *et al.*[35] indeed showed that the Yb^{3+} ions can enter 8*h* and 4*e* square-antiprism sites noted Yb1 and Yb2. The observed groups of levels thus could be associated with these two types of sites and slight distortions of them. Knowing that the corresponding local site symmetry is close to C_{4v} (Refs. 13 and 14) and that the average Yb-F distances in the square antiprisms (eight F^- ions at 2.3 Å and one F^- ion at 2.9 Å) are close to that found for the isolated centers of tetragonal symmetry (eight F^- ions at 2.3 Å and one F^- ion at 2.73 Å), other groups of electronic energy levels should be found with similar crystal-field splittings. Inspecting again Figs. 8 and 15 and disregarding the peaks occurring around 10 384 and 10 849 cm^{-1}, which are due to the cubic centers, and the bumps occurring around 10 630 and 10 870 cm^{-1}, which are assigned according to Raman spectra to vibronic sidebands associated with local phonons of 420 and 695 cm^{-1}, two groups of weak lines appear around 10 300 and 10 580 cm^{-1}. These lines thus likely correspond to transitions to excited energy levels at about 100 and 380 cm^{-1} above the lowest Stark component of the $^2F_{5/2}$ multiplet. Such weak lines and crystal-field splittings are indeed very close to that found for the C_{4v} isolated centers (see in Figs. 3 and 4). Correlatively, groups of emission lines should be found corresponding to transitions down to ground-state Stark components at higher energies than the ones already identified around 50 cm^{-1}. Inspecting again Figs. 9 and 15, one group of lines indeed occurs around 10 080 cm^{-1} and another one around 9660 cm^{-1}. This indicates groups of levels around 110 and 530 cm^{-1}, the latter being superimposed but clearly different from the above mentioned vibronic sideband.

It is thus concluded to the existence of groups of energy levels located around 0, 50, 100, and 530 cm^{-1} for the ground multiplet $^2F_{7/2}$ and around 10 200, 10 300, and 10 580 cm^{-1} for the $^2F_{5/2}$ metastable one. Such an interpretation is relatively close to that proposed by Voron'ko *et al.*[38] but greatly differ from that given by Ito *et al.*[39] This is due, as mentioned above, to confusions with some lines coming from the cubic centers and with some vibronic sidebands. It is worth mentioning at the end that if the multisite character of the optical transitions pertaining to the hexameric clusters is clearly seen at low temperature, the corresponding structures progressively broaden with the temperature to reach a common homogeneously broadened profile.

V. CONCLUSION

Spectroscopic measurements have been made at low as well as high temperatures with high quality crystals made of very pure raw materials, grown in oxygen-free atmosphere, and doped with various amounts of Yb^{3+} ions from about 0.03 to 25 at. % Yb^{3+}. These measurements have confirmed first, at low dopant concentrations, the existence of three kinds of Yb^{3+} isolated centers corresponding to cubic, tetragonal, and trigonal local site environments. The pure electronic energy levels of each of these Yb^{3+} centers have been clearly identified and found to be in rather good agreement with the crystal-field calculations. These measurements have also proved that when the Yb^{3+} concentration is higher than about 0.05 at. % and does not exceed about 8–10 at. %, a unique type of Yb^{3+} luminescent center appears and progressively dominates over all the previous ones. Following the experimentally derived energy-level positions as well as the EXAFS structural data which can be found in the literature, such a luminescent and lasing center is likely made of a cubo-octahedral hexameric cluster in which the six Yb^{3+} ions site in square antiprisms of nearly tetragonal site symmetry. Of course, depending on the crystal-growth procedure and at very high dopant concentrations, the hexameric arrangement may change more or less significantly, resulting in slightly different spectral profiles and emission lifetimes. This may be the reason why some authors have found slightly different data from ours.

*Corresponding author:patrice.camy@ensicaen.fr

[1] W. J. Humphreys, Astrophys. J. **20**, 266 (1904).
[2] M. G. Urbain, Ann. Chim. Phys. **18**, 222 (1909).
[3] D. C. Stockbarger, J. Opt. Soc. Am. **39**, 731 (1949).
[4] W. Hayes, *Crystal with the Fluorite Structure: Electronic, Vibrational, and Defect Properties*, The International Series of Monographs on Physics (Clarendon, Oxford, 1974).
[5] C. R. A. Catlow, A. V. Chadwick, G. N. Greaves, and L. M. Moroney, Nature (London) **313**, 601 (1984).
[6] J. Corish, C. R. A. Catlow, P. W. M. Jacobs, and S. H. Ong, Phys. Rev. B **25**, 6425 (1982).
[7] N. M. Strickland and G. D. Jones, Phys. Rev. B **56**, 10916 (1997).
[8] Jon-Paul R. Wells and R. J. Reeves, Phys. Rev. B **64**, 035102 (2001).
[9] V. Petit, P. Camy, J.-L. Doualan, and R. Moncorgé, J. Lumin. **122-123**, 5 (2007).
[10] P. J. Bendall, C. R. A. Catlow, J. Corish, and P. W. Jacobs, J. Solid State Chem. **51**, 159 (1984).
[11] S. E. Ness, D. J. M. Bevan, and H. J. Rossell, Eur. J. Solid State Inorg. Chem. **25**, 509 (1988).
[12] D. J. M. Bevan, M. J. C. McCall, S. E. Ness, and M. R. Taylors, Eur. J. Solid State Inorg. Chem. **25**, 517 (1988).
[13] A. E. Nikiforov, A. Yu. Zakharov, M. Yu. Ugryumov, S. A. Kazanski, A. I. Ryskin, and G. S. Shakurov, Phys. Solid State **47**, 1431 (2005)
[14] S. A. Kazanskii, A. I. Ryskin, A. E. Nikiforov, A. Y. Zaharov, M. Y. Ougrumov, and G. S. Shakurov, Phys. Rev. B **72**, 014127

(2005).
[15] V. Petit, J. L. Doualan, P. Camy, V. Ménard, and R. Moncorgé, Appl. Phys. B: Lasers Opt. **78**, 681 (2004).
[16] A. Lucca, M. Jacquemet, F. Druon, F. Balembois, P. Georges, J. L. Doualan, P. Camy, and R. Moncorgé, Opt. Lett. **29**, 1879 (2004).
[17] A. Lucca, G. Debourg, M. Jacquemet, F. Druon, F. Balembois, P. Georges, P. Camy, J. L. Doualan, and R. Moncorgé, Opt. Lett. **29**, 2767 (2004).
[18] R. Czarny, M. Alouini, X. Marcadet, S. Bansropun, J. L. Doualan, R. Moncorgé, J. F. Lampin, M. Krakowski, and D. Dolfi, IEEE International Topical Meeting on Microwave Photonics, Piscataway, NJ, 2006 (unpublished), Catalog No. 06EX1314, pp. 290–2.
[19] M. Siebold, M. Hornung, S. Bock, J. Hein, M. C. Kaluza, J. Wemans, and R. Uecker, Appl. Phys. B: Lasers Opt. **89**, 543 (2007).
[20] A. Pugzlys, D. Sidorov, T. Ali, A. Baltuska, L. Su, J. Xu, R. Li, L. Giniunas, and R. Danielis, Advanced Solid State Photonics, Nara, Japan, January 2008 (unpublished), OSA Technical Digest Paper No. MF4.
[21] M. L. Falin, K. I. Gerasimov, V. A. Latypov, A. M. Leushin, H. Bill, and D. Lovy, J. Lumin. **102-103**, 239 (2003).
[22] U. Ranon and A. Yaniv, Phys. Lett. **9**, 17 (1964).
[23] W. Low, Phys. Rev. **118**, 1608 (1960); Phys. Lett. **26A**, 234 (1968).
[24] M. J. Weber and R. W. Bierig, Phys. Rev. **134**, 1492 (1964).
[25] R. W. Bierig, M. J. Weber, and S. I. Warshaw, Phys. Rev. **134**, 1504 (1964).
[26] S. D. McLaughlan and R. C. Newman, Phys. Lett. **19**, 552 (1965).
[27] S. D. McLaughlan, P. A. Forrester, and A. F. Fray, Phys. Rev. **146**, 344 (1966).
[28] J. Kirton and S. D. McLaughlan, Phys. Rev. **155**, 279 (1967).
[29] M. L. Falin, K. I. Gerasimov, V. A. Latypov, and A. M. Leushin, Appl. Magn. Reson. **26**, 617 (2004).
[30] U. Ranon and J. S. Hyde, Phys. Rev. **141**, 259 (1966).
[31] J. M. Baker, W. B. J. Blake, and G. M. Copland, Proc. R. Soc. London, Ser. A **309**, 119 (1969).
[32] J. M. Baker and W. B. J. Blake, Proc. R. Soc. London, Ser. A **316**, 63 (1970).
[33] D. Kiro and W. Low, Phys. Rev. Lett. **20**, 1010 (1968).
[34] C. A. Ramos, C. Fainstein, and M. Tovar, Phys. Rev. B **32**, 64 (1985).
[35] J. P. Laval, A. Abaouz, B. Frit, and A. Le Bail, J. Solid State Chem. **85**, 133 (1990).
[36] W. Low, J. Chem. Phys. **37**, 30 (1962).
[37] J. Kirton and A. M. White, Phys. Rev. **178**, 543 (1969).
[38] Yu. K. Voron'ko, V. V. Osiko, and I. A. Shcherbakov, Sov. Phys. JETP **29**, 86 (1969).
[39] M. Ito, C. Goutaudier, Y. Guyot, K. Lebbou, T. Fukuda, and G. Boulon, J. Phys.: Condens. Matter **16**, 1501 (2004).
[40] V. Petit, Ph.D. thesis, Université de Caen, 2006.
[41] J. M. Baker and E. R. Davies, J. Phys. C **8**, 1870 (1975).
[42] S. H. Choh, J. Phys. C **10**, 1413 (1977).
[43] E. Friedman and W. Low, J. Chem. Phys. **33**, 1275 (1960).
[44] F. Min-Tsong Lay and A. W. Nolle, Phys. Rev. **163**, 266 (1967).
[45] D. N. Chambers and R. C. Newman, J. Phys. C **4**, 517 (1971).
[46] A. Ferrier, M. Velázquez, and R. Moncorgé, Phys. Rev. B **77**, 075122 (2008).
[47] C. A. Morrison and R. P. Leavitt, J. Chem. Phys. **71**, 2366 (1979).
[48] C. Li, C. Wyon, and R. Moncorgé, IEEE J. Quantum Electron. **28**, 1209 (1992).